nature communications

Article

https://doi.org/10.1038/s41467-024-53103-w

Ultrafast dynamics evidence of strong coupling superconductivity in $LaH_{10\pm\delta}$

Received: 4 February 2024

Accepted: 30 September 2024

Published online: 08 November 2024

Check for updates

Y. L. Wu[1,2,6], X. H. Yu[1,3,4,6], J. Z. L. Hasaien[1,3,6], Fang Hong[1,3] ✉, P. F. Shan[1,3], Z. Y. Tian[1], Y. N. Zhai[1,3], J. P. Hu[1,3,5], J. G. Cheng[1,3] ✉ & Jimin Zhao[1,3,4] ✉

Recently, tremendous research interest has been aroused in clathrate superhydrides. However, their microscopic properties, especially the superconducting (SC) gap and electron-phonon coupling (EPC) strength, are largely unexplored experimentally. Here, we investigate the time-resolved ultrafast spectroscopy of a superconductor $LaH_{10\pm\delta}$ under an ultrahigh pressure of 165 GPa. By analyzing the ultrafast dynamics of the quasiparticles, we experimentally obtain the SC gap $\Delta(0) = 53 \pm 5$ meV, revealing a gap ratio $2\Delta(0)/k_BT_c = 5.6$ and a gap parameter $\vartheta = 1.95$. Significantly, we experimentally estimate $\lambda\langle\Omega^2\rangle = (2.4 \pm 0.1) \times 10^4$ $(meV)^2$, which corresponds to an EPC strength $\lambda = 2.58 \pm 0.11$. These results together provide direct experimental evidence that strong EPC is responsible for the near-room-temperature superconductivity in clathrate superhydrides. Our investigation significantly advances the experimental exploration of superhydrides, and contributes to the ultrafast dynamics investigations of quantum materials under high pressures.

The recent advances in hydrogen-rich superconductors[1–8] with near-room-temperature superconductivity has aroused tremendous research interest[9–17]. After the exciting experimental discovery of superconductivity in sulfur hydride with a superconducting (SC) transition temperature $T_c = 203$ K[18], a large family of theoretically predicted clathrate-type metal superhydrides[1–4,7,9] were subsequently synthesized and confirmed to superconduct with near-room-temperature T_c values[5,6,8–13,19–21]. Among the known clathrate superhydrides, $LaH_{10\pm\delta}$ exhibits the highest T_c of 250–260 K under pressures of 165–190 GPa[5,6,20].

To date, the experimental investigations on the SC properties and mechanisms of these clathrate superhydrides are mainly via electrical transport measurements, owing to the limited small sample size (typically of 5–10 μm) when using diamond anvil cell (DAC) to endow an ultrahigh pressure (>150 GPa) condition. Other experimental explorations, such as Meissner effect[22–24], X-ray diffraction[5,12,22], Raman scattering[25], etc., only emerge recently.

There have rarely been reports on spectroscopy investigations on the clathrate superhydrides, leaving the microscopic SC pairing mechanism of their superconductivity almost unexplored experimentally. Particularly, direct experimental evidence of strong electron-phonon coupling (EPC) responsible for the high-T_c superconductivity in these clathrate superhydrides is still lacking to date. Furthermore, experimental observation of the SC gap in clathrate superhydrides has rarely been reported. These leave the theoretical predictions of a strong EPC based on the BCS mechanism not directly verified experimentally.

Spectroscopy experiments (e.g., infrared spectroscopy, ultrafast spectroscopy, scanning tunneling spectroscopy, angle-resolved photoelectron spectroscopy, neutron spectroscopy, Raman spectroscopy,

[1]Beijing National Laboratory for Condensed Matter Physics, Institute of Physics, Chinese Academy of Sciences, Beijing, China. [2]Hebei Key Laboratory of Microstructural Material Physics, School of Science, Yanshan University, Qinhuangdao, China. [3]School of Physical Sciences, University of Chinese Academy of Sciences, Beijing, China. [4]Songshan Lake Materials Laboratory, Dongguan, Guangdong, China. [5]New Cornerstone Science Laboratory, Beijing, China. [6]These authors contributed equally: Y. L. Wu, X. H. Yu, J. Z. L. Hasaien. ✉e-mail: hongfang@iphy.ac.cn; jgcheng@iphy.ac.cn; jmzhao@iphy.ac.cn

etc.) under megabar pressures will be challenging[26,27] owing to the limited sample space and size, sample quality, pressure uniformity, two-beam alignment, laser heating[15,23], etc. Hence, more effective spectroscopy experimental means are urgently needed to investigate such quantum materials under ultrahigh pressure conditions.

Ultrafast pump-probe spectroscopy has ultrahigh time resolution and unique capability of exploring non-equilibrium states far above the Fermi surface[28–31], especially in high temperature superconductors[31–33]. Recently, on-site in situ high-pressure ultrafast spectroscopy has been developed to investigate high pressure ultrafast dynamics[26,27], which achieved the capability of precisely measuring both the amplitude and lifetime of the quasiparticles (QPs), enabling it to probe the SC phase transitions. However, to date there has been no reports on ultrafast dynamics investigations of quantum materials under an ultrahigh pressure.

In this work, we successfully combine co-linear microscopic ultrafast pump-probe spectroscopy with ultrahigh pressure and with low temperature technology (see Methods), with which reliable ultrahigh pressure ultrafast dynamics data (in both amplitudes and lifetimes) are achieved. The SC gap and EPC strength are both experimentally obtained. Consequently, we have discovered experimental evidence for the strong-coupling nature of SC mechanism in clathrate superhydrides.

Results

Varying temperature ultrafast dynamics of $LaH_{10\pm\delta}$ at 165 GPa

We measure the photo-induced relative differential reflectivity ΔR/R of our $LaH_{10\pm\delta}$ sample (see Methods). The experimental setup is similar to the on-site in situ high pressure ultrafast system we recently innovated[26,27], except that here the DAC is cooled to low temperatures, with the high pressure remaining constant. The sample is anchored in a DAC (inset of Fig. 1), whose photograph is shown in Supplementary Fig. 1. Figure 1 illustrates a typical time-resolved scanning trace of such an ultrafast relaxation process at 190 K and 165 GPa, ranging from −3 to 140 ps. It is well known that |ΔR/R| is proportional to the density of photo-excited QPs (see Methods).

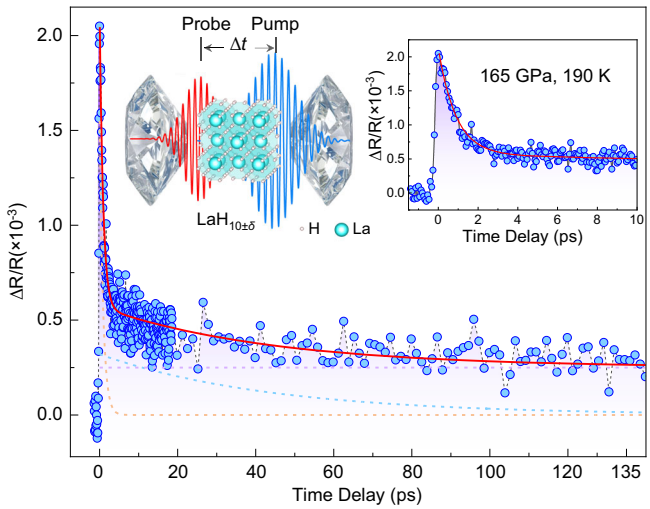

Fig. 1 | Typical ultrafast dynamics scanning trace at 165 GPa and 190 K. The relaxation results are fitted by a three-exponential function (red solid curve), which is decomposed into the fast (yellow curve), slow (blue curve), and slowest (purple curve) components. These three processes are more distinctly seen by a log-scale presentation in Supplementary Fig. 2. Left panel inset: schematic details of the ultrahigh pressure ultrafast light-matter interaction encapsulated in the DAC. The crystal structure of $LaH_{10\pm\delta}$ is schematically shown, sandwiched in between a pair of diamonds. The two-color pump and probe light pulses are also depicted, between which the time interval Δt is scanned. Right panel inset: temporal zoom-in view of the ultrafast dynamics signal, revealing the initial fast relaxation process.

Following the convention[32,33], the data are quantitatively analyzed by employing a fitting equation $f(t) = \Delta R/R(t) = A_{fast}\exp(-t/\tau_{fast}) + A_{slow}\exp(-t/\tau_{slow}) + A_0$, where A_{fast}, A_{slow} and A_0 denote the amplitudes of the QP relaxation, and τ_{fast} and τ_{slow} are the QP lifetimes. Deconvolution of the data is conducted to account for the finite temporal duration of the light pulse, with $[f \otimes g](t) \equiv \int_{-\infty}^{+\infty} f(\xi)g(t-\xi)d\xi$, where $g(t) = \frac{1}{\sigma\sqrt{\pi}}e^{-t^2/\sigma^2}$ is a Gaussian function with a width $FWHM = 2\sqrt{\ln 2}\sigma$[34]. The fitting result is plotted in Fig. 1 as a red solid curve, which is fully consistent with the experimental data. A more distinctive identification of the three components is presented in Supplementary Fig. 2 by using a logarithmic plotting. The three components are plotted as dashed curves in Fig. 1: the fast component (yellow curve) is attributed to EPC, the slow component (blue curve) is ascribed to phonon-phonon scattering (e.g., anharmonic decay of optical phonons into acoustic phonons), and the constant term (purple line) is assigned to heat diffusion involving acoustic phonons[31,35] with a much longer lifetime at the order of 1 ns.

The temperature dependence data of the ultrahigh-pressure ultrafast dynamics are shown in Fig. 2. Both the amplitudes and lifetimes of the QP relaxation vary significantly with temperature (Fig. 2a). Figure 2b illustrates the normalized data, which better reveals the gradually varying lifetimes with temperature. To qualitatively identify whether there is a SC phase transition, we plot a color map of the ΔR/R signals (Fig. 2a) in Fig. 2c. Two distinct color regions can be identified, reflecting the dynamic variations in the density and lifetime of the photo-excited carriers. The color change at 220 K qualitatively indicates a possible SC transition. We also re-measure the resistance of our $LaH_{10\pm\delta}$ sample upon increasing temperature (the same as for our ultrafast dynamics measurement) without external field right before our ultrafast spectroscopy experiment, which is plotted as the blue curve in Fig. 2c. The likely SC transition temperature we observe in the ultrafast spectroscopy is consistent with the re-measured transport result, manifesting that the sample still well-preserves its SC properties, and the slight lowering of the T_c as compared with ref. 20 can be attributed to the long-time-caused slight relaxation.

Obtaining the SC gap Δ(0), gap ratio $2\Delta(0)/k_BT_c$, and gap parameter ϑ

Quantitatively, the temperature dependence data of the dynamics are analyzed, which yields the fitting parameters A_{fast}, τ_{fast}, A_{slow}, and τ_{slow}, as summarized in Fig. 3. While the fast component varies in a regular way with temperature, the slow component exhibits salient features. The A_{fast} exhibits a regular decrease that can be seen in many quantum materials, and the τ_{fast} is nearly a constant, reflecting a constant EPC strength. We will discuss how we quantitatively obtain the EPC strength λ from τ_{fast} in a later paragraph, together with the varying fluence experimental results. The A_{slow} experiences a sharp decrease with temperature at 150–220 K. Simultaneously, for the same temperature region, τ_{slow} first decreases then exhibits a dramatic enhancement with temperature near 220 K. The two characteristic temperatures coincide with each other, exhibiting an identical $T_c = 220$ K, which manifests the well-known phonon bottleneck effect[27,32,33,36–39]. Such simultaneous critical behaviors in both amplitude and lifetime of the slow component correspond to a gap closing at the critical temperature.

We use the Rothwarf-Taylor model[40] and its extended derivation[33,36] to fit the temperature dependence of A_{slow} and τ_{slow}, which is a multi-process model based on SC gap and Cooper pairs. The amplitude and lifetime of the slow component are depicted by $A_{slow}(T) = \Upsilon[\sqrt{\Delta(T)T}\exp(-\Delta(T)/k_BT) + C]^{-1}$ and $\tau_{slow}(T) = \{\Gamma[\delta + 2n_T(T)][\Delta(T) + \alpha T\Delta(T)^4]\}^{-1}$, where $n_T \propto \sqrt{\Delta(T)T}\exp(-\Delta(T)/k_BT)$ is the density of the equilibrium thermal QPs, $\Delta(T) = \Delta(0)\tanh(\vartheta\sqrt{T_c/T-1})$ is the empirical trial SC gap function[41], k_B is the Boltzmann constant, ϑ is a parameter reflecting the correlation

https://doi.org/10.1038/s41467-024-53103-w

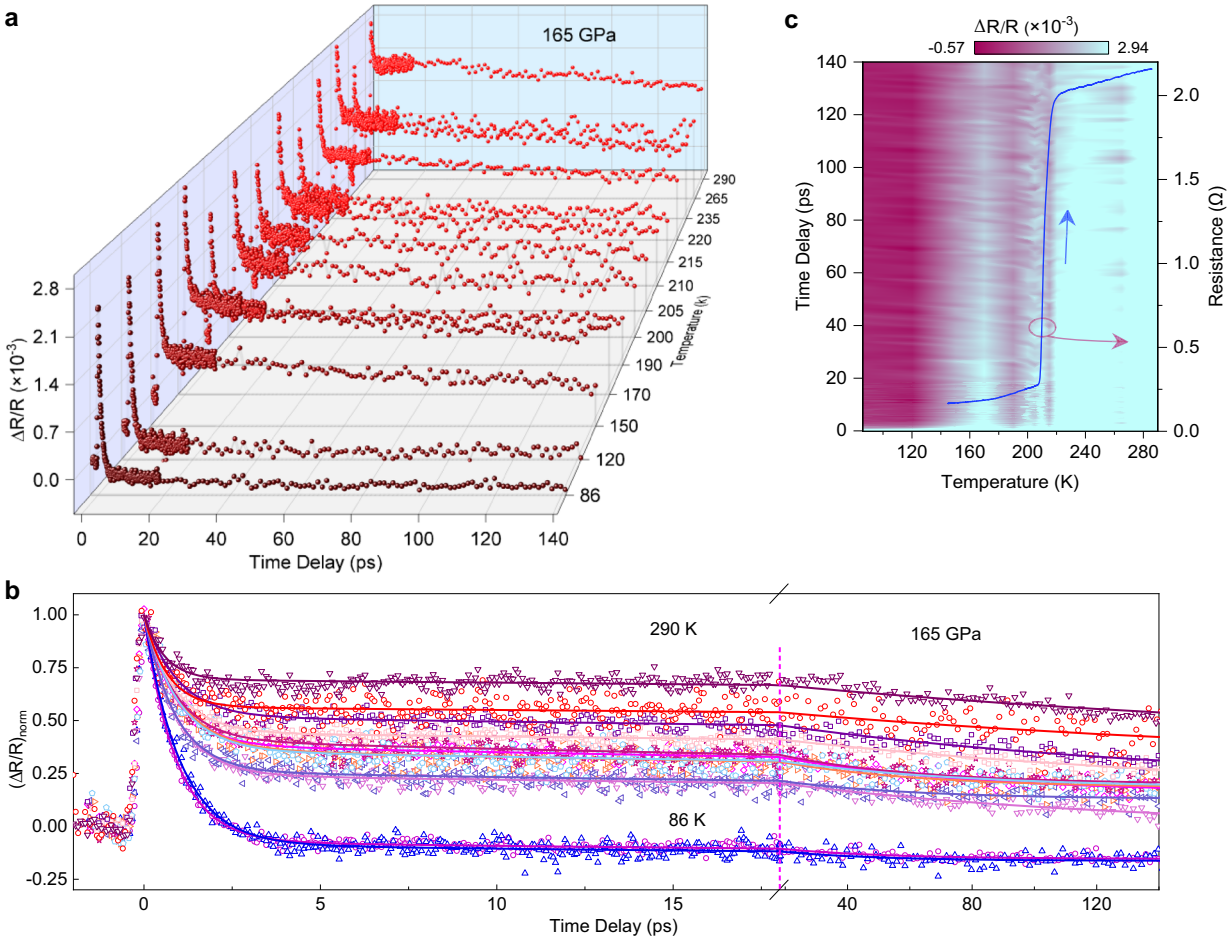

Fig. 2 | Low temperature ultrahigh pressure ultrafast QP dynamics of $LaH_{10\pm\delta}$. **a** Relative differential reflectivity scanning traces at different temperatures. Both the amplitudes and lifetimes vary with temperature. **b** Normalized ΔR/R of the data in **a** clearly manifesting the variation in lifetimes. For clarity, the initial dynamics (from −2 to 18 ps) and the longer-range dynamics (from 18 to 140 ps) are separated by a dashed line. Solid curves: fittings using three-component functions. **c** Color map of the ΔR/R data in **a** as a function of both delay time and temperature. Blue curve: temperature-dependent resistance of the $LaH_{10\pm\delta}$ sample during a warming up process. The SC T_c qualitatively exhibited and that from the transport measurement are in line with each other.

strength. Here, the Υ, Γ, ϑ, C, Δ(0), α, and δ are all independent fitting parameters (for their physical essence and the detailed data fitting procedure, see Supplementary Information). In Fig. 3c, d the experimental data are fitted well (red curves) and the SC transition is clearly discernable. Explicitly, we obtain the SC $T_c = 219 \pm 4$ K and SC gap $\Delta(0) = 53 \pm 5$ meV. This experimentally observed SC gap value is reasonably consistent with the theoretically predicted value (e.g., 62 meV at 170 GPa in ref. 42). Considering the long-time relaxation of the ultrahigh pressure sample after months, the SC T_c value is also reasonably consistent with the original 250 K T_c value[20]. Importantly, no pre-specified coefficient is set between Δ(0) and T_c; thus, the values are obtained independently in our spectroscopic experiment. With the observed values, we obtain a gap ratio of $2\Delta(0)/k_BT_c = 5.6$, which is clearly above the BCS weak-coupling ratio 3.5, and is consistent with the theoretical value of 5.54 at 170 GPa[42]. By fitting the slow component (Fig. 3c, d), we obtain $\vartheta = 1.95$, where by convention $\vartheta > 1.74$ corresponds to a strong-coupling BCS gap[41]. Therefore, both the gap ratio and gap parameter ϑ lead us to conclude that we have evidenced a strong-coupling BCS gap in $LaH_{10\pm\delta}$. In addition, we also obtain an empirical expression for the temperature-dependent SC gap, $\Delta(T) = \Delta(0)\tanh(1.95\sqrt{T_c/T-1})$, which has not been previously reported for near-room temperature superconductors.

The variation feature at 120–150 K (Fig. 3c, d) has rarely been observed in superconductors under ambient pressure. Both the quality and fitting of the time-domain data are good, as explicitly shown in Supplementary Figs. 3 and 4. The temperature dependence of the static reflectivity R exhibits no feature at 120–150 K (see Supplementary Fig. 5). Our transport measurement shows no feature at 120–150 K either[20]. We do not know the exact origin of this feature. Several possible explanations can be thought of. The feature could be due to some extrinsic change of the DAC; It could also be that the sample is a mixed multi-phase crystal—the sample may not be so uniform; Even a second SC phase could also be possible to potentially account for the feature at 120–150 K. Note that this feature occurs far away from the SC T_c; thus, the discussion does not affect our understanding of the superconductivity.

Obtaining the EPC strength from the fast component lifetime

Furthermore, we measure the fluence dependence of the ultrafast relaxation signals at 78 K (see Methods), for which the results are shown in Fig. 4. As expected, the transient dynamics strongly depend on the laser fluence (Fig. 4a), qualitatively exhibiting a proportional relation. For the normalized scanning traces (Fig. 4b), the log-scale figure clearly reveals the different relaxation channels, where the fast and slow components are clearly identified. In Fig. 4c, the experimental data $|\Delta R/R|_{max}$ are very well fitted by a linear relation, manifesting the transient differential reflectivity is proportional to the photo-excited carrier density. It spans from 0 to 6.2 mJ/cm^2, fully covering the 5.0 mJ/cm^2 working fluence for harvesting the data in Fig. 3, which demonstrates that the thermal effects are

https://doi.org/10.1038/s41467-024-53103-w

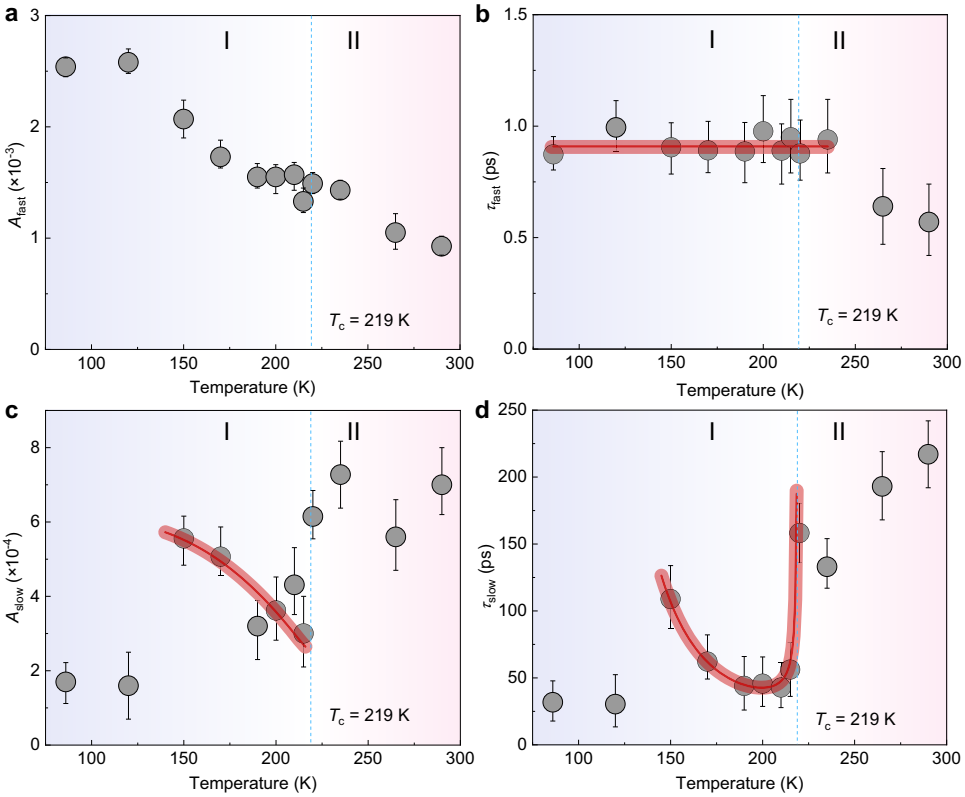

Fig. 3 | Temperature dependence of the fast and slow components of the QP relaxation dynamics. a, **b** Amplitude A_{fast} and lifetime τ_{fast} of the fast component. The A_{fast} decreases with increasing temperature, which is regular for quantum materials. The τ_{fast} is nearly a constant, reflecting a constant electron-phonon coupling strength. The slight decrease at above 250 K may be due to some lattice structure relaxation. **c**, **d** Amplitude A_{slow} and lifetime τ_{slow} of the slow component. Both A_{slow} and τ_{slow} exhibit a feature near an identical critical temperature T_c: A_{slow} experiences a decrease with increasing temperature, reaching a minimum value near T_c = 219 K; τ_{slow} first decreases, then increases dramatically when approaching the same T_c. Solid curves in **c**, **d**: fitting curves using the RT model. I and II mark the SC and normal phases, respectively. Color background: a guide to the eyes for the SC phase transition. Temperature dependence of the A_0 term is discussed in Supplementary Fig. 6. The error bars represent the fitting errors.

negligible[33,43–45] although the sample is small. For each experiment, linear dependence on fluence (or power) needs to be tested to ensure there is no laser heating (see Methods and Supplementary Information). Such linear dependence reflects there is no Coulomb blockade or renormalization in the electronic bands, allowing the Fermi golden rule and RT model to apply.

Significantly, we quantitatively investigate the EPC strength λ based on the direct experimental observation of the ultrafast dynamics of $LaH_{10\pm\delta}$, particularly by measuring τ_{fast}. Usually, one needs to know the specific heat coefficient (i.e., Sommerfeld parameter) and the light penetration depth at the excitation wavelength of the material[32,33]. For $LaH_{10\pm\delta}$ under ultrahigh pressure, these two physical properties are not reported so far, owing to the lack of experimental investigations. Nevertheless, it has been demonstrated that these obstacles can be circumvented by temperature-dependence or fluence-dependence experimental results[35,46], by regarding the specific heat coefficient and penetration depth as constant fitting parameters. Extending the phenomenological Allen relation $1/\tau_{fast} = 3\hbar\lambda\langle\Omega^2\rangle/\pi k_B T_e$[47] to its temperature dependence version, we have[35] $\tau_{fast} = \frac{\pi k_B\sqrt{\Theta F}}{3\hbar\lambda\langle\Omega^2\rangle}(1+\frac{T_L^2}{2\Theta F})$, where $\lambda\langle\Omega^2\rangle$ is the second moment of the Eliashberg function, Θ is a parameter determined by the reflectivity, optical penetration depth, and specific heat coefficient (see Supplementary Information), F is the pump fluence, T_L is the lattice temperature (i.e., environmental temperature), λ is the EPC strength, and Ω is the phonon frequency. Fitting the temperature-dependent τ_{fast} data in Fig. 3b using this relation, we obtain a red solid curve (Fig. 3b), yielding an EPC strength of $\lambda\langle\Omega^2\rangle \approx 2.45\times10^4$ (meV)^2. Note that the slight decrease in τ_{fast} at $T > 250$ K may be due to some lattice structural relaxation. In parallel, the fluence-dependence experimental data are carefully analyzed by employing the three-exponential decaying function aforementioned, of which the fitting parameters A_{fast}, τ_{fast}, A_{slow}, and τ_{slow} are summarized in Fig. 4d, e. Extending the Allen's relation to the fluence dependence version[46], and later on the fluence dependence version at a given temperature[35], we have $\tau_{fast} = \frac{\pi k_B^2\sqrt{T_L^2+\Theta F}\left(\sqrt{T_L^2+\Theta F}-T_L\right)}{3\hbar^2\langle\Omega^3\rangle\left[\frac{1}{e^{\hbar\langle\Omega\rangle/k_B\sqrt{T_L^2+\Theta F}}-1}-\frac{1}{e^{\hbar\langle\Omega\rangle/k_B T_L}-1}\right]}$. By fitting the experimentally measured lifetime data τ_{fast} in Fig. 4d (red curve), we obtain $\lambda\langle\Omega^2\rangle \approx 2.3\times10^4$ (meV)^2, which is fairly consistent with the value we obtained above. The consistency between the two methods corroborates the reliability of the EPC value we obtain. Here, we adapt an averaged value $\lambda\langle\Omega^2\rangle = (2.4\pm0.1)\times10^4$ (meV)^2 in our further discussion (for details, see Supplementary Information). This value is in line with all the reported theoretical predictions with explicitly calculated values nearby 165 GPa[7,9,48] (see Supplementary Table 1). Following the convention[49], we substitute Ω by the logarithmic frequency average Ω_{log} in $\lambda\langle\Omega^2\rangle$. Taking Ω_{log} = 96.4 meV at 163 GPa[7], we estimate $\lambda = 2.58\pm0.11$ for $LaH_{10\pm\delta}$ under 165 GPa, which is in good agreement with the theoretical value of $\lambda = 2.67$ in ref. 7. Therefore, our ultrahigh-pressure ultrafast dynamics investigation provides a unique crucial experimental evidence of strong coupling superconductivity in clathrate superhydride superconductors. We have also performed a separate control experiment to repeat the whole set of experiments, including fabricating a new $LaH_{10\pm\delta}$ sample and re-perform the high-pressure ultrafast spectroscopy experiments,

https://doi.org/10.1038/s41467-024-53103-w

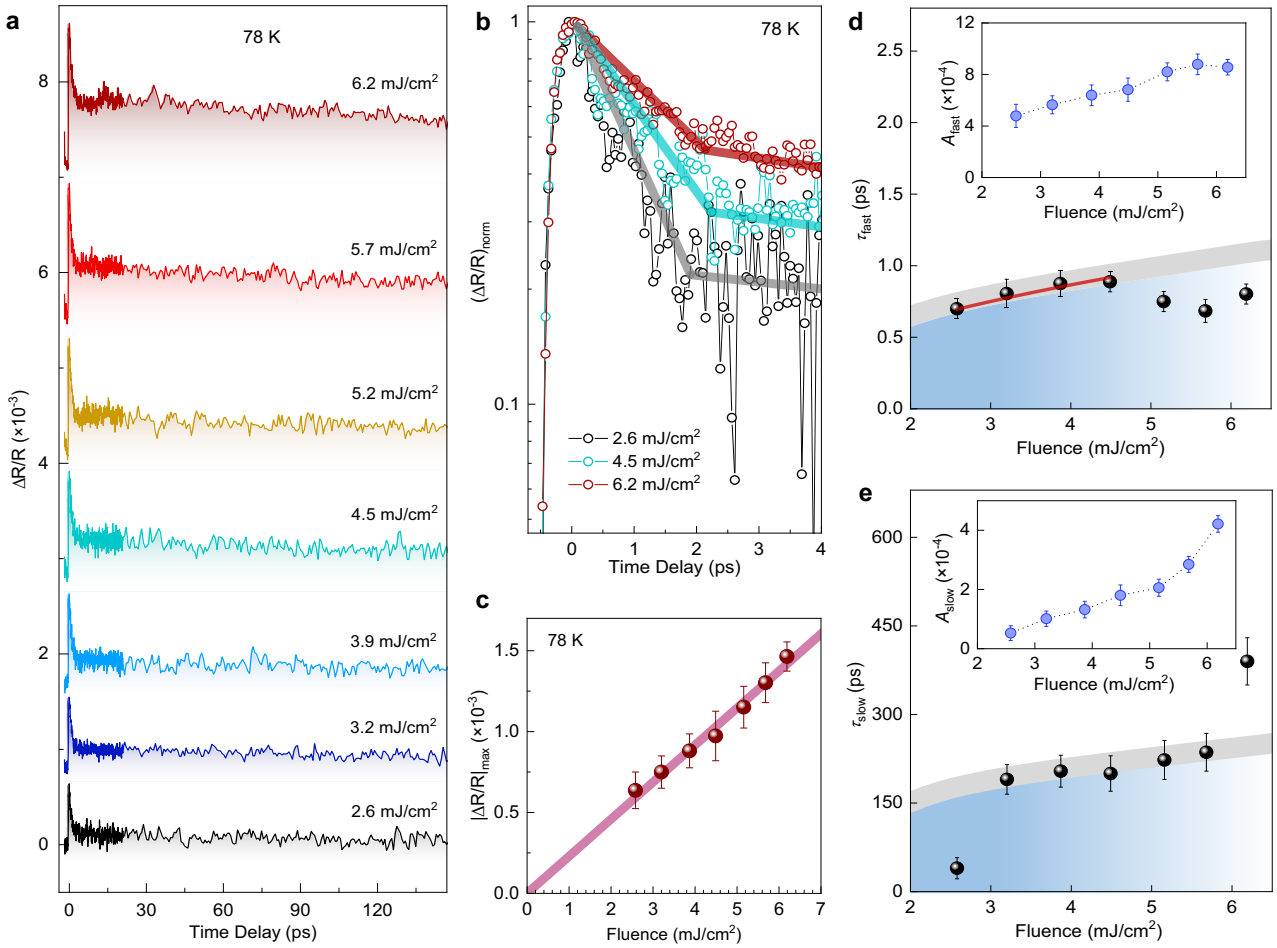

Fig. 4 | Fluence-dependence of the high-pressure ultrafast dynamics in $LaH_{10\pm\delta}$. **a** Time-resolved transient signal ΔR/R under different pump fluences at 78 K (offset for clarity), which exhibits a prominent enhancement upon increasing fluence. **b** Normalized ΔR/R at fluences of 2.6, 4.5, and 6.2 mJ/cm², respectively, displaying the temporal zoom-in view of the initial dynamics. The *y*-axis is in log-scale, clearly revealing the fast and slow components, each marked by a line segment. **c** Pump fluence dependence of $|\Delta R/R|_{max}$ near the so-called time-zero, where the solid line is a linear fit to the data. The linear fluence dependence without saturation clearly shows that there is no thermal effect. **d** Lifetime τ_{fast} and amplitude A_{fast} of the fast component. τ_{fast} slightly increases with fluence at below 4.5 mJ/cm², corresponding to a constant EPC strength λ[35,46]. For fluences larger than 4.5 mJ/cm², τ_{fast} slightly decreases due to saturation. In the inset, A_{fast} steadily increases with fluence, reflecting the increase in excited state carrier density. **e** Lifetime τ_{slow} and amplitude A_{slow} of the slow component. τ_{slow} overall slightly increases with fluence, and A_{slow} increases steadily with fluence. The combined trends in A_{fast} and A_{slow} are consistent with the result in **c**. The A_0 component is also investigated, which remains a constant with increasing fluence (see Supplementary Fig. 6b). The error bars in **c** represent the measurement fluctuation. The error bars in **d**, **e** denote the fitting errors.

as well as data analysis. Overall, the results are in line with the data we presented above (for details, see Supplementary Information).

Conclusion

In conclusion, we have developed a low-temperature ultrahigh-pressure ultrafast pump-probe spectroscopy technique to investigate the excited state QP ultrafast dynamics of $LaH_{10\pm\delta}$ at 165 GPa. We directly measure that the SC gap is $\Delta(0) = 53 \pm 5$ meV and the EPC strength is $\lambda = 2.58 \pm 0.11$, which provide a unique experimental evidence for the long-sought strong coupling superconductivity in clathrate superhydrides. Moreover, a gap ratio of $2\Delta(0)/k_BT_c = 5.6$ and a gap parameter of $\vartheta = 1.95$ are also experimentally obtained, both corroborating the strong-coupling characteristic of $LaH_{10\pm\delta}$. Our results greatly advance the experimental understanding about the SC mechanism of the near-room temperature superconductivity. Our investigation greatly boosts the field of high-pressure ultrafast science, which can be extended to other near-room temperature superconductors and other quantum materials. Thus, we foresee the dawn of a promising unexplored frontier area, which canvasses extensive investigations of non-equilibrium quantum states under high pressures.

Methods

Ultrahigh-pressure ultrafast pump-probe spectroscopy experiment

The experimental setup is similar to the on-site in situ high pressure ultrafast system we recently innovated (see refs. 26,27), except that here the DAC is cooled down to liquid nitrogen temperature in an open cycle continuous flow cryostat. During the whole experiment, the high pressure in the DAC is kept constant. Two-color ultrahigh pressure femtosecond pump-probe spectroscopy experiment has been carried out, with a pulse duration of 70 fs, using a 250 kHz optical parametric amplifier system to reduce the thermal effect. Our temperature-dependence experiment is carried out from liquid nitrogen to room temperature. The wavelengths of the pump and probe beams are 620 and 800 nm, the powers are 200 and 60 μW, the $1/e^2$ beam diameters are 4.5 and 4.3 μm, and the fluences are 5.0 and 1.6 mJ/cm², respectively. Note that, during the experiment, the chopper blocks a half of the pump power (i.e., the 200 μW power is reduced to 100 μW), which actually reduces the potential thermal effect (the same is true for the fluence dependence experiment). For the fluence dependence experiment, the pump and probe wavelengths are 650 and 800 nm, respectively; the pump power varies

from 100 to 240 μW, and the probe power is kept at 40 μW; the $1/e^2$ pump and probe beam diameters are 4.4 and 2.5 μm, respectively; the pump fluence varies from 2.6 to 6.2 mJ/cm^2 and the probe fluence is fixed at 3.2 mJ/cm^2.

For both the temperature-dependence and fluence-dependence ultrafast experiments, cross-polarization detection geometry is implemented to reduce interference. An optical cage system is constructed in the light path to reduce the fluctuations of the laser spot position on the sample surface. In our experiment, the influence of the static reflectivity R (Supplementary Fig. 5) is excluded by measuring the relative differential reflectivity ΔR/R.

It is well known that |ΔR/R| is proportional to the density of photo-excited QPs and the process is described by the Fermi Goden Rule. The pump pulse incidents on the sample surface, which promotes the ground-state electrons to the excited state far above the Fermi surface. As the pump pulse propagates away, the photo-excited none-quilibrium state carriers relax back to the ground state due to the EPC and phonon-phonon interactions, which is detected by the probe pulse with controlled scanning delay time.

Technical breakthroughs for ultrahigh-pressure ultrafast spectroscopy

Several major challenges have been overcome in our experiment. First, low temperature and varying temperature experiments are needed for our investigation, which is prominently more challenging than our recently achieved room temperature high-pressure ultrafast spectroscopy instrumentation and experiment[26,27]. The cooling down and warming up of the whole DAC take much longer time (e.g., $t > 1.5$ h) for each of the temperature point, especially because for such an ultrahigh pressure experiment the frame of the DAC is made of steel. Second, the DAC cell needs to be compatible with the low temperature cryostat. Particularly, thermal sensor needs to be anchored as close as possible to the sample and highly transparent optical window is needed. Third, the sample size is as small as 10×20 μm^2 due to the ultrahigh-pressure synthesis and experiment. Consequently, microscopic ultrafast spectroscopy experiment has to be implemented. Thus, relatively strong laser beam has to be avoided due to the tight focusing and weak signal detection is needed. Forth, because an objective lens has to be used, co-linear geometry has to be implemented, making it more challenging to remove the unfavorable interference between the pump and probe beams. Fifth, two-color experiment thus has to be implemented. Diamonds have strong absorptions in the ultraviolet wavelength range[50]. As a result, we avoid the much easier 400–800 nm laser wavelength setup and choose to implement the tunable visible light. Overall, based on the above five aspects of technical breakthroughs, our method is challenging in implementing a two-beam low temperature high-pressure ultrafast pump-probe experiment[26] and has the advantage of employing much smaller laser spot sizes, ensuring probing the sample itself without any interference from the electrodes, substrates, and other parts (Supplementary Fig. 1).

Origin of the positive-negative sign in ultrafast spectroscopy

Ultrafast pump-probe spectroscopy usually employs lock-in amplifiers, which contain an internal reference signal when detecting the real signal. There is a reference phase shift between the reference signal and input signal, which can be adjusted by pressing the auto-phase button on the front panel of the lock-in amplifier. This will introduce an overall positive or negative sign upon the scanning trace. By moving the motorized linear stage to a location with negative value, pressing the auto-phase button, then doing the scan again, the whole new scanning curve will be flipped, like being multiplied by a negative sign. In such a way, whether the peak is upward or downward can be easily controlled by the electronics. This electronic phase is additional to the input signal from the sample. This sign is different from the sign change (at different wavelength) due to real absorption. Such an overall sign needs to be decided at the beginning of the whole set of experiment, and should not be changed during the latter-on measurements. In our experiments, we do the "auto-phase" only at the beginning and do not do it again throughout the entire experiment.

In general, the pump beam might enhance or reduce the reflectivity of a sample. Hence, the sign of the pump-probe data can be calibrated, such as by using a reference sample under intense pump and probe beams, without involving the chopper and lock-in electronic phase. Here, due to the lack of a reference sample, we did not carry out this calibration, which will not affect the conclusions in this work.

Evidence and criteria of no thermal effect in ultrafast spectroscopy

Although an objective lens is used in the pump-probe light paths and the laser spots are as small as a few microns on the sample surface, the repetition rate is low (250 kHz), and the total power (~0.1 mW) in this experiment is much lower than those in a regular pump-probe experiment. Hence the thermal effect is effectively avoided. It has been well known that laser heating is more prominent at lower temperatures and higher repetition rate excitations. Here, the temperature is relatively high (around 220 K), and the repetition rate is low (250 kHz, much lower than 80 MHz), which further confirms that there are no thermal effects (i.e., no laser heating) in our experiment. Indeed, for thermal effect, the total power in pump and probe beams is more crucial than the fluences, because thermal effects are due to accumulated heat, which is mainly related to the laser power input and heat dissipation by cooling. The most reliable and widely accepted criteria that there is no thermal effect is that the $|\Delta R/R|_{max}$ signal is linearly proportional to the pump laser fluence[33].

Sample preparation

Our $LaH_{10\pm\delta}$ sample was synthesized at 165 GPa ultrahigh pressure and 1700 K high temperature, with a lateral size of 10×20 μm^2, for which the details are described in ref. 20. The characteristic onset transition temperature T_c of our $LaH_{10\pm\delta}$ sample was initially determined to be 240–250 K by the transport measurement[20]. The re-measured transition temperature is depicted in the main text. The symmetry of the lattice structure of $LaH_{10\pm\delta}$ has been previously identified to be $Fm\bar{3}m$, using XRD measurements, where the $Fm\bar{3}m$ phase were found to be a stable phase under an ultrahigh pressure of 138–170 GPa[5,6,22,51].

Data availability

The data that support the findings of this study are available from the corresponding author upon request. The source data underlying Figs. 2 and 4 are provided as a Source Data file. Source data are provided with this paper.

References

1. Ashcroft, N. W. Hydrogen dominant metallic alloys: high temperature superconductors? *Phys. Rev. Lett.* **92**, 187002 (2004).
2. Wang, H., Tse, J. S., Tanaka, K., Iitaka, T. & Ma, Y. Superconductive sodalite-like clathrate calcium hydride at high pressures. *Proc. Natl Acad. Sci. USA* **109**, 6463–6466 (2012).
3. Liu, H., Naumov, I. I., Hoffmann, R., Ashcroft, N. W. & Hemley, R. J. Potential high-T_c superconducting lanthanum and yttrium hydrides at high pressure. *Proc. Natl Acad. Sci. USA* **114**, 6990–6995 (2017).
4. Peng, F. et al. Hydrogen clathrate structures in rare earth hydrides at high pressures: possible route to room-temperature superconductivity. *Phys. Rev. Lett.* **119**, 107001 (2017).
5. Drozdov, A. P. et al. Superconductivity at 250 K in lanthanum hydride under high pressures. *Nature* **569**, 528–531 (2019).
6. Somayazulu, M. et al. Evidence for superconductivity above 260 K in lanthanum superhydride at megabar pressures. *Phys. Rev. Lett.* **122**, 027001 (2019).

7. Errea, I. et al. Quantum crystal structure in the 250-kelvin superconducting lanthanum hydride. *Nature* **578**, 66–69 (2020).
8. Kong, P. et al. Superconductivity up to 243 K in the yttrium-hydrogen system under high pressure. *Nat. Commun.* **12**, 5075 (2021).
9. Salke, N. P. et al. Synthesis of clathrate cerium superhydride CeH_9 at 80-100 GPa with atomic hydrogen sublattice. *Nat. Commun.* **10**, 4453 (2019).
10. Li, X. et al. Polyhydride CeH_9 with an atomic-like hydrogen clathrate structure. *Nat. Commun.* **10**, 3461 (2019).
11. Semenok, D. V. et al. Superconductivity at 161 K in thorium hydride ThH_{10}: synthesis and properties. *Mater. Today* **33**, 36–44 (2020).
12. Ma, L. et al. High-temperature superconducting phase in clathrate calcium hydride CaH_6 up to 215 K at a pressure of 172 GP. *Phys. Rev. Lett.* **128**, 167001 (2022).
13. Li, Z. et al. Superconductivity above 200 K discovered in superhydrides of calcium. *Nat. Commun.* **13**, 2863 (2022).
14. Gor'kov, L. P. & Kresin, V. Z. Colloquium: high pressure and road to room temperature superconductivity. *Rev. Mod. Phys.* **90**, 011001 (2018).
15. Flores-Livas, J. A. et al. A perspective on conventional high-temperature superconductors at high pressure: methods and materials. *Phys. Rep.* **856**, 1–78 (2020).
16. Zhang, L., Wang, Y., Lv, J. & Ma, Y. M. Materials discovery at high pressures. *Nat. Rev. Mater.* **2**, 17005 (2017).
17. Pickett, W. E. Colloquium: room temperature superconductivity: the roles of theory and materials design. *Rev. Mod. Phys.* **95**, 021001 (2023).
18. Drozdov, A. P., Eremets, M. I., Troyan, I. A., Ksenofontov, V. & Shylin, S. I. Conventional superconductivity at 203 kelvin at high pressures in the sulfur hydride system. *Nature* **525**, 73–76 (2015).
19. Chen, W. H. et al. Enhancement of superconducting properties in the La-Ce-H system at moderate pressures. *Nat. Commun.* **14**, 2660 (2023).
20. Hong, F. et al. Superconductivity of lanthanum superhydride investigated using the standard four-probe configuration under high pressures. *Chin. Phys. Lett.* **37**, 107401 (2020).
21. Capitani, F. et al. Spectroscopic evidence of a new energy scale for superconductivity in H_3S. *Nat. Phys.* **13**, 859 (2017).
22. Minkov, V. S. et al. Magnetic field screening in hydrogen-rich high-temperature superconductors. *Nat. Commun.* **13**, 3194 (2022).
23. Struzhkin, V. et al. Superconductivity in La and Y hydrides: remaining questions to experiment and theory. *Matter Radiat. Extremes* **5**, 028201 (2020).
24. Minkov, V. S., Ksenofontov, V., Bud'ko, S. L., Talantsev, E. F. & Eremets, M. I. Magnetic flux trapping in hydrogen-rich high-temperature superconductors. *Nat. Phys.* **19**, 1293 (2023).
25. Purans, J. et al. Local electronic structure rearrangements and strong anharmonicity in YH_3 under pressures up to 180 GPa. *Nat. Commun.* **12**, 1765 (2021).
26. Wu, Y. L. et al. On-site in situ high-pressure ultrafast pump–probe spectroscopy instrument,. *Rev. Sci. Instrum.* **92**, 113002 (2021).
27. Wu, Y. L., Yin, X., Hasaien, J. Z. L., Ding, Y. & Zhao, Jimin High-pressure ultrafast dynamics in Sr_2IrO_4: pressure-induced phonon bottleneck effect. *Chin. Phys. Lett.* **37**, 047801 (2020).
28. Orenstein, J. Ultrafast spectroscopy of quantum materials. *Phys. Today* **65**, 44–50 (2012).
29. Kirilyuk, A., Kimel, A. V. & Rasing, T. Ultrafast optical manipulation of magnetic order. *Rev. Mod. Phys.* **82**, 2731 (2010).
30. Basov, D. N., Averitt, R. D. & Hsieh, D. Towards properties on demand in quantum materials. *Nat. Mater.* **16**, 1077–1088 (2017).
31. Giannetti, C. et al. Ultrafast optical spectroscopy of strongly correlated materials and high-temperature superconductors: a non-equilibrium approach. *Adv. Phys.* **65**, 58–238 (2016).
32. Tian, Y. C. et al. Ultrafast dynamics evidence of high temperature superconductivity in single unit cell FeSe on $SrTiO_3$. *Phys. Rev. Lett.* **116**, 107001 (2016).
33. Wu, Q. et al. Ultrafast quasiparticle dynamics and electron-phonon coupling in $(Li_{0.84}Fe_{0.16})OHFe_{0.98}Se$. *Chin. Phys. Lett.* **37**, 097802 (2020).
34. Hilton, D. J. & Tang, C. L. Optical orientation and femtosecond relaxation of spin-polarized holes in GaAs. *Phys. Rev. Lett.* **89**, 146601 (2002).
35. Tian, Z. Y. et al. Ultraweak electron-phonon coupling strength in cubic boron arsenide unveiled by ultrafast dynamics. *Phys. Rev. B* **105**, 174306 (2022).
36. Kabanov, V. V., Demsar, J. & Mihailovic, D. Kinetics of superconductor excited with a femtosecond optical pulse. *Phys. Rev. Lett.* **95**, 147002 (2005).
37. Gedik, N., Blake, P., Spitzer, R. C. & Orenstein, J. Single-quasiparticle stability and quasiparticle-pair decay in $YBa_2Cu_3O_{6.5}$. *Phys. Rev. B* **70**, 014504 (2004).
38. Chia, E. E. M. et al. Quasiparticle relaxation across the spin-density-wave gap in the itinerant antiferromagnet $UNiGa_5$. *Phys. Rev. B* **74**, 140409(R) (2006).
39. Sun, F. et al. Spin-polarized gap in the magnetic Weyl semimetal $Co_3Sn_2S_2$. *Phys. Rev. B* **104**, L100301 (2021).
40. Rothwarf, A. & Taylor, B. N. Measurement of recombination lifetimes in superconductors. *Phys. Rev. Lett.* **19**, 27 (1967).
41. Gross, F. et al. Anomalous temperature dependence of the magnetic field penetration depth in superconducting UBe_{13}. *Z. Phys. B Condens. Matter* **64**, 175–188 (1986).
42. Kruglov, I. A. et al. Superconductivity of LaH_{10} and LaH_6 polyhydrides. *Phys. Rev. B* **101**, 024508 (2020).
43. Gedik, N. et al. Abrupt transition in quasiparticle dynamics at optimal doping in a cuprate superconductor system. *Phys. Rev. Lett.* **95**, 117005 (2005).
44. Giannetti, C. et al. Discontinuity of the ultrafast electronic response of underdoped Superconducting $Bi_2Sr_2CaCu_2O_{8+\delta}$ strongly excited by ultrashort light pulses. *Phys. Rev. B* **79**, 224502 (2009).
45. Torchinsky, D. H. et al. Nonequilibrium quasiparticle relaxation dynamics in single crystals of hole- and electron-doped $BaFe_2As_2$. *Phys. Rev. B* **84**, 104518 (2011).
46. Wu, Qiong et al. Quasiparticle dynamics and electron-phonon coupling in Weyl semimetal TaAs. *Phys. Rev. Mater.* **4**, 064201 (2020).
47. Allen, P. B. Theory of thermal relaxation of electrons in metals. *Phys. Rev. Lett.* **59**, 1460 (1987).
48. Semenok, D. V. et al. Effect of magnetic impurities on superconductivity in LaH_{10}. *Adv. Mater.* **34**, 2204038 (2022).
49. Allen, P. B. & Dynes, R. C. Transition temperature of strong-coupled superconductors reanalyzed. *Phys. Rev. B* **12**, 905 (1975).
50. Clark, C. D., Ditchburn, R. W. & Dyer, H. B. The absorption spectra of natural and irradiated diamonds. *Proc. R. Soc. Lond. A* **234**, 363–381 (1956).
51. Sun, D. et al. High-temperature superconductivity on the verge of a structural instability in lanthanum superhydride. *Nat. Commun.* **12**, 6863 (2021).

Acknowledgements

This work was supported by the National Key R&D Program of China (Grants No. 2021YFA1400201 J.Z., 2017YFA0303603 J.Z., 2022YFA140390 J.P.H., 2023YFA1608900 X.H.Y., 2021YFA1400300 F.H.), CAS Project for Young Scientists in Basic Research (Grant No. YSBR-059 J.Z.), Strategic Priority Research Program of CAS (Grants No. XDB30000000 J.Z., XDB33000000 X.H.Y.), National Natural Science Foundation of China (Grants No. 12025408 J.G.C., 11574383 J.Z., 12204400 Y.L.W.), International Partnership Program of Chinese Academy of Sciences (Grant No. GJHZ1826 J.Z., GJTD–2020-01 J.G.C.), Beijing Natural Science Foundation (4191003 J.Z.), CAS

Interdisciplinary Innovation Team (J.Z.), and New cornerstone investigator program (J.P.H.).

Author contributions

J.Z. conceived the idea and supervised the project. Y.L.W., J.Z.L.H., and J.Z. conducted the low-temperature ultrahigh pressure ultrafast pump-probe spectroscopy experiment with assistance from Z.Y.T. and Y.N.Z.; X.H.Y., F.H., P.F.S., and J.G.C. prepared the samples and characterized resistance. Y.L.W. and J.Z. analyzed the data. J.Z., J.G.C., and J.P.H. discussed the results. J.Z. wrote the paper with inputs from J.G.C. and all authors.

Competing interests

The authors declare no competing interests.

Additional information

Supplementary information The online version contains supplementary material available at https://doi.org/10.1038/s41467-024-53103-w.

Correspondence and requests for materials should be addressed to Fang Hong, J. G. Cheng or Jimin Zhao.

Peer review information *Nature Communications* thanks the anonymous reviewers for their contribution to the peer review of this work. A peer review file is available.